Acta Materialia 102 (2016) 304–314

Contents lists available at ScienceDirect

Acta Materialia

journal homepage: www.elsevier.com/locate/actamat

Solid solution strengthening of hexagonal titanium alloys: Restoring forces and stacking faults calculated from first principles

P. Kwasniak*, H. Garbacz, K.J. Kurzydlowski

Materials Design Division, Faculty of Materials Science and Engineering, Warsaw University of Technology, Woloska 141, 02-507 Warsaw, Poland

ARTICLE INFO

Article history:
Received 4 May 2015
Received in revised form
20 September 2015
Accepted 21 September 2015
Available online xxx

Keywords:
Titanium alloys
Ab initio calculations
Ductility
Stacking faults

ABSTRACT

The solid solution strengthening of α-Ti was investigated in respect of dislocation nucleation and dissociation in all four active glide modes. A series of Ti+X alloys (X = Al, Sn, V, Zr and O) was selected to analyze the impact of solute valence structure (Al, Sn – *p* type elements, V, Zr – *d* type elements) and lattice site (interstitial O) on the mechanisms responsible for variation of mechanical properties. The computational procedure relied on the generalized stacking fault energy (GSFE) concept combined with the nudged elastic band method that enables full atomic relaxation and determination of the true, minimum energy GSFE path. Additionally, various concentrations of solutes and their distance to the glide plane were considered as well. Our study revealed a strong, nonlinear influence of X position on GSFE and migration of O atoms during the crystal slip. These new phenomena allowed one to determine three solution strengthening mechanisms: (I) hindrance of <*a*> prismatic dislocation emission and reconfiguration of 1/3 <11$\bar{2}$0> screw dislocation cores (*p* type solutes), (II) hindrance of <*a*> prismatic dislocation emission (V) and SFE reduction in other modes (both *d* type solutes) and (III) suppression of dislocation nucleation in all modes caused by O. We found that the stacking faults formed by the single partial dislocations have a thickness of few atomic layers and exhibit a highly non-uniform structure. Their ability to accommodate the lattice deformation introduced by solute elements greatly affects the stacking fault energies of the α-Ti alloys.

1. Introduction

The high strength-to-density ratio of hcp Ti and Mg makes them valuable for all spheres of industry in which reduction of energy consumption and weight play a major role. The development of metallurgy, processing and solid state physics related with their properties are of particular interest. One of the method for improvement of mechanical properties of Mg and Ti is solution strengthening. Further investigation of solution effects in these metals is motivated by the enormous ductility enhancement in Mg–Y alloys [1] and high strength with balanced malleability in Ti–O systems [2] both occurring in single phase alloys.

Plastic deformation in α-Ti can be realized by four types of slip systems on three glide planes [3]: <11$\bar{2}$0> (0001) – <*a*> on the basal plane, I <11$\bar{2}$0> {10$\bar{1}$0} – <*a*> on prismatic plane, II <11$\bar{2}$0> {10$\bar{1}$1} – <*a*> on pyramidal plane, I <11$\bar{2}$3> {10$\bar{1}$1} – <*c*+*a*> on pyramidal plane (I and II symbols indicate larger and smaller interplanar distance, respectively [4]). The fifth deformation mode is twinning. The activity of these systems has been studied for decades, resulting in the description of several solution strengthening concepts. A strong chemical impact of alloying elements on deformation modes was postulated by Conrad, Collings and co-workers [5,6] who categorized the alloying elements into two groups: B-type, with *p* valence structure radically improving strength, and T2 group consisting of transition metals with a markedly weaker strengthening effect. Distinct mechanical properties of Ti–B and Ti-T2 alloys were explained by large perturbation of the electronic wave functions caused by *p* elements resulting in strong bonds character similar to those occurring in intermetallic TiAl phase. It is worth noting that interstitial elements like C, H, N and O which have the most prominent impact on α-Ti properties [6] were classified as B solutes and their different lattice positions were not analyzed. Separate interstitials effect was investigated by the measurements of critical resolved shear stresses (CRSS) in α-Ti. Churchman [7] observed that O and N change relative activity of glide modes and proposed simple lattice model, denoting dependency between particular slip systems and the number of

* Corresponding author.
E-mail address: piotr.kwasniak@inmat.pw.edu.pl (P. Kwasniak).

http://dx.doi.org/10.1016/j.actamat.2015.09.041
1359-6454/

Ti–O(N) bonds broken during the slip. Further, the selective impact of substitutional solutes on deformation modes was also confirmed by Zaeffer [8] who showed a conspicuous increase in the amount of basal dislocations and reduction of the CRSS <c+a> pyramidal/<a> prism ratio in TiAl6V4 alloy relative to pure Ti.

Progress in our understanding of the generalized stacking fault energy (GSFE or γ) [9–15] and development of the computational methods like density functional theory (DFT) [16] allowed for detailed analysis of titanium plasticity. Complex calculation of the α-Ti GSFE [4] revealed the existence of stable stacking fault (SF) configurations in all slip systems. The interplay of interstitial O with some of these faults was examined in Refs. [17,18] with the conclusion that O stabilizes/destabilizes basal/prismatic faults, respectively. The next important feature of the planar defects – twin boundaries (TB) reported lately [19], show better solubility of many Ti alloying atoms in TB than in bulk. This unique phenomenon was correlated with the excess TB volume delocalized within 4–5 atomic planes, implying relatively large TB – solute interaction distance. It should also be noted that appropriate modification of the γ curve calculation procedure [4] makes it possible to precisely determine the restoring forces of dislocations nucleation in all α-Ti slip systems. However, comprehensive GSFE studies of Ti based alloys are still unavailable.

Another valuable approach to α-Ti ductility relies on full dislocations modeling using DFT and molecular dynamic (MD) techniques. Low temperature deformation of titanium is controlled by the motion of 1/3<11$\bar{2}$0> prism screw dislocations [8,20–22]. The privileged activity of these dislocations compared to basal glide in IV B elements (Ti, Zr, Hf) originates from the low prism SF energy [23,24]. The 1/3<11$\bar{2}$0> core structure is still a matter of debate [25–28], but its five distinct geometries have been distinguished. Different cores are identified as strain spreading into various atomic planes, leading to local SF configurations. The lowest energy 1/3<11$\bar{2}$0> core is planar and predominantly spread on the prism plane [26,27]. However, other configurations are partially spread on the prism, basal and pyramidal planes with only ~0.004–0.006 eV/*b* energy excess [27]. These results are consistent with the polymorphism of dislocation cores confirmed experimentally in MgO [29]. The calculations made for other materials indicate that dislocation core geometry and Peierls potential can be altered by alloying elements [30]. Direct interaction of the solute atoms with dislocation cores (rather than its elastic interaction at a finite distance) has been also proposed as a main strengthening mechanism in α-Ti [20,21].

Summarizing, it has been shown that α-Ti solution strengthening is deeply related with the solute valence structure, its position in the crystal lattice and interaction with structural defects. While deformation by twining is relatively well described, knowledge about dislocation nucleation and motion in Ti alloys is still very limited. The available reports show great capabilities of DFT in terms of dislocation nucleation prediction [4] and the substantial impact of alloying elements on SF stability [17,18], which in turn control the structure and mobility of dislocation cores [23,26,27]. Both restoring forces and SF energies of Ti alloys can be accurately determined by the GSFE calculations, and their changes are fundamental for understanding the solution strengthening mechanism.

In this paper we present a systematic study of the GSFE calculated by the first principle approach for all active slip systems in a series of hexagonal Ti+X alloys. X = Al, Sn, V, Zr and O were selected to determine the effect of the valence structure and lattice position of solutes on the characteristics of γ curves. Additionally, two concentrations of alloying elements and their interaction were analyzed. The results obtained demonstrate unexpected oxygen migration forced by the crystal slip and significant, nonlinear variations of the γ curves as a function of the slip plane – solute atom distance for all studied elements in most slip modes. These new effects together with other results and available experimental data were discussed in terms of dislocation nucleation and possible dislocation core structure modification in the studied alloys.

2. Computational method

Ab initio calculations were performed using Vienna *Ab initio* Simulation Package (VASP) code [31,32], with the projector augmented wave (PAW) method for core-valence electron interaction [33]. Our previous studies [34,35] showed that Perdew-Burke-Ernzerhof (PBE) [36] generalized gradient functional properly reproduce properties of Ti and Ti-based alloys, and therefore was utilized in this study. The number of valence electrons for pseudopotentials used in computations are as follows: 3 for Al ($3s^2$, $3p^1$), 4 for Sn ($5s^2$, $5p^2$), 6 for O ($2s^2$, $2p^4$), 4 for Ti ($3d^2$, $4s^2$), 5 for V ($3d^3$, $4s^2$) and 12 for Zr ($4s^2$, $4p^6$, $4d^2$, $5s^2$).

Fermi smearing of the electronic occupancy with 0.2 eV and plane-wave cutoff energy of 425 eV was used. The Brillouin zone was sampled in accordance with the Monkhorst-Pack scheme [37]. The suitable 16 × 16 × 12 k-point mesh for α-Ti unit cell was initially established and subsequently adjusted to the investigated slab models. The relaxation of ions was stopped when 1 and 20 meV/Å force (for equilibrium and distorted structures, respectively) and 1 meV energy convergences were reached. These parameters allowed one to obtain very good agreement of lattice constants $a = 2.94$ Å and $c/a = 1.583$ with experiments $a = 2.95$ Å and $c/a = 1.587$ [38]. According to the slip planes available in α-Ti (prismatic, basal and pyramidal) three types of supercells were built. Preliminary γ curve computations were performed to establish the correct geometry of the models with respect to the number of atomic planes, their size and vacuum height.[1] Finally, 18 atomic layer models (4 atoms in each plane – 2 × 2 in-plane unit cell) with 8, 12, and 10 Å of free space, respectively, for basal, prism, and pyramidal slip modes were chosen for full GSFE calculations. In the alloyed systems one solute atom (substitutional or interstitial) was placed in each supercell. The selected models ensure GSFE errors less than 5% relative to twice as high reference structures (36 planes). Two types of larger structures were also adopted:

(I) 3 × 3 in-plane unit cell, 18 atomic layers supercells used when alloying element concentration was analyzed,
(II) 2 × 2 in-plane unit cell, 26 atomic layers structures utilized for calculations of X–SF effective range interaction. The results obtained for larger models are explicitly marked in the text.

The GSFE reproduces the interplanar potential energy for sliding one-half of a rigid crystal over the other half along the glide plane. According to this definition the output energy variation is equal to a pure misfit energy of particular slip planes. Since, the atomic relaxation in conventional γ curve computations is allowed only in direction perpendicular to the glide plane the measured misfit energy is not precise. It is expected that the additional “in-plane” atomic shuffling should reduce GSFE by varying slip amplitude and

[1] Our tests showed no differences of pure Ti GSFEs when atomic plane areas are equal to or higher than 2 × 2 unit cell (the SFE, USFE and maximum gradients of γ curve reach errors up to 3% between 1 × 1, 2 × 2, 3 × 3 and 4 × 4 plane size). However, we found energy gradient errors of up to 10% for the single unit cell plane size at the onset of the slip. To eliminate this issue, further improvement of k-points density and NEB force convergence criterion for the smallest structures are required. This modification substantially increases calculation time without any significant γ corrections observed in the larger supercells.

crystal distortion from single to several atomic planes. The fully relaxed γ curves are possible to calculate employing, the nudged elastic-band method (NEB) [39,40]. The NEB is a minimum energy path (MEP) finding tool for transitions between known initial and final states. The great advantage of this approach is the possibility to perform all-dimension relaxations of metastable systems. Previous calculations performed for pure α-Ti [4] revealed that the GSFE slip trajectories (MEP) are non-straight, with pronounced curvature observed in pyramidal modes. Additionally, atomic displacements above and below glide planes during the slip are large, achieving one half of the Burgers vector length. These significant distortions lead to a noticeable reduction of GSFE in many of α-Ti slip modes [4].

In this study we used the NEB method to calculate GSFE in all α-Ti slip modes. The γ curves resolution depends on the Burgers vector length and slip geometry (from 9 to 18 finite displacement steps). The first (bottom) atomic plane in each model was frozen to prevent crystal drift generating spurious forces. Utilizing the rigid GSFE concept, the fault vector is chosen arbitrarily, while in the NEB approach, the motion of each atom is an output of calculations. Owing to the fact that all non equilibrium energy contributions (energy needed to break the atomic bonds and elastic strain energy) originate from the misfit of the slipping atomic planes, the fault vector in the presented methodology is equal to the 3D trajectory of the Ti atoms located in the first atomic plane of the upper (slipping) part of the crystal. Since the structure transition in the NEB method is expressed with respect to reaction coordinates and GSFE provides energy as a function of fault vector length, the distances between sampling points at γ (NEB) curves may be non equidistant. However, careful NEB parameterization (number of images and force convergence criterion) is required for accurate results of energy gradients and continuous transition trace. To avoid the rigid γ drawbacks [4] we used the climbing image nudged elastic band (CI-NEB) method [41] allowing one to compute γ curves along the unconstrained path of crystal slips with precise values of saddle points. Global force NEB optimizations (instead of image by image) were performed with limited-memory Broyden–Fletcher–Goldfarb–Shanno, fast inertial relaxation engine and quick-min ionic optimizers [39] depending on the Hellmann–Feynman force values.

3. Results and discussion

3.1. Restoring forces and stacking faults

GSFE of hexagonal Ti+X alloys calculated with 2×2 in-plane unit cell models (total X concentration about 1.4 at%) and various distances (d_X) between X and slip planes are shown in Fig. 1. It is generally accepted that unstable stacking fault energy γ_{USF} (global maximum of the γ curves) is a measure of the energy barrier for dislocation emission [42], whereas stacking fault energy γ_{SF} (local γ minimum) indicates the existence of metastable structures formed during crystal slip, essential for dislocation dissociation. The γ curves of pure titanium indicate the existence of a metastable SF configuration in each slip system, which is in accordance with previous calculations [4]. The computed γ_{SF} values are also consistent with available data for basal[2] and prism modes (Table 1). Nevertheless, a few important facts arising from the alloyed α-Ti GSFE characteristics should be highlighted. Firstly, the distance d_X greatly affects the γ curves. As an example, an Sn atom located directly below the shifted part of the crystal in prism modes does not change γ shape while for the next Sn positions (one and two atomic planes below the glide plane) both γ_{USF} and γ_{SF} values are markedly different (Fig. 1). Moreover, of all the slip systems only basal slip exhibits a linear relation between d_X and γ – the larger d_X the γ variations are smaller. Secondly, apart from a few prismatic and pyramidal exceptions, substitutional solutes essentially do not improve γ_{USF} indicating that the energy barrier for dislocations emission for alloyed systems are in fact similar to pure Ti. This result is unexpected, since all solutes analyzed here improve the strength of α-Ti [6]. A similar trend was noticed recently in many Mg alloys [46], implying that the solution strengthening of hcp metals may have a common origin. The most important variations of γ curves plotted in Fig. 1 are related with γ_{SF} which is reduced mainly in basal mode. It is important to note that the addition of alloying elements may also destabilize SF configurations occurring in pure Ti e.g. <a> prism Ti+Sn(+1), <a> pyramidal Ti+V(+1,+2).

The influence of interstitial O on GSFEs of α-Ti is much stronger than any substitutional element considered in this work. Oxygen significantly improves γ_{USF} values in all slip modes, especially in basal and prismatic slip. However, this explicit effect is visible only when the O atom is located directly in the glide plane whereas for larger d_X distances the strengthening is almost fully reduced (Fig. 1). The distinct impact of O on γ_{USF} emerges from structure transformation to SF geometry and may be elucidated based on Fig. 2. An initial octahedral site is transformed to tetra- or hexahedral [47,48] ones after partial dislocation emission in the basal plane – local fcc structure is generated. The crystal rearrangement forces O to migrate into a newly formed octahedral position at the intermediate step of the slip. An analogous transition also occurs in other <a> type glide modes, but the final SF structure and available interstitial site are different. The only system that maintains the initial O position is <c+a> pyramidal mode, which requires layer-by-layer collective crystal slip for interstitial site deformation.

As seen in Fig. 2b, the obtained slip trajectories of Ti atoms are continuous and consistent with previous DFT results [4]. Nonetheless, the distance between some O positions is noticeable. Crystal slip results in the continuous “closing” and “opening” of the original and new interstitial sites along the glide planes. O changes its position at critical stage of the slip when the Ti–O bonds are interrupted. The jump to the new “open” interstitial site is instantaneous and proceeds along almost a straight line. The climbing image technique [41] allows to find the energy barriers (γ_{USF}) of the considered modes, which are usually correlated with an energy barrier for O shuffling (in Ti+O systems). It should be emphasized that increased number of NEB images does not change the energy gradient or USFE, indicating the absence of any energetically important intermediate O positions. This new phenomenon is similar to model presented by Oberson et al. [49,50] who showed that lattice reorientation during α- and β-Ti twining eliminates octahedral sites leading to O diffusion. An additional non-equilibrium interstitial site in prism SF was also illustrated by M. Ghazisaeidi et al. [18]. Very recent, extensive investigations of the oxygen strengthening effect in α+Ti demonstrate the intense pinning effect of O on screw prismatic dislocations [51] and confirm experimentally the new O interstitial site located in prism stacking faults, which are equivalent to the position determined in this study. Although previous works took into account only selected slip modes, the frozen O position or stationary SF configurations without elastic conversion from the initial structure presented here, they confirm our predictions. The strengthening effect of O consists in its shuffling to a non equilibrium interstitial site available at SF configuration. Details of metastable SF geometries and the interstitial O position in all slip modes are given in the next section.

[2] All basal faults considered in this study are intrinsic I_2 type faults formed by the $1/3<10\bar{1}0>$ partial dislocation emission resulting in the basal plane stacking sequence: ABABCACA….

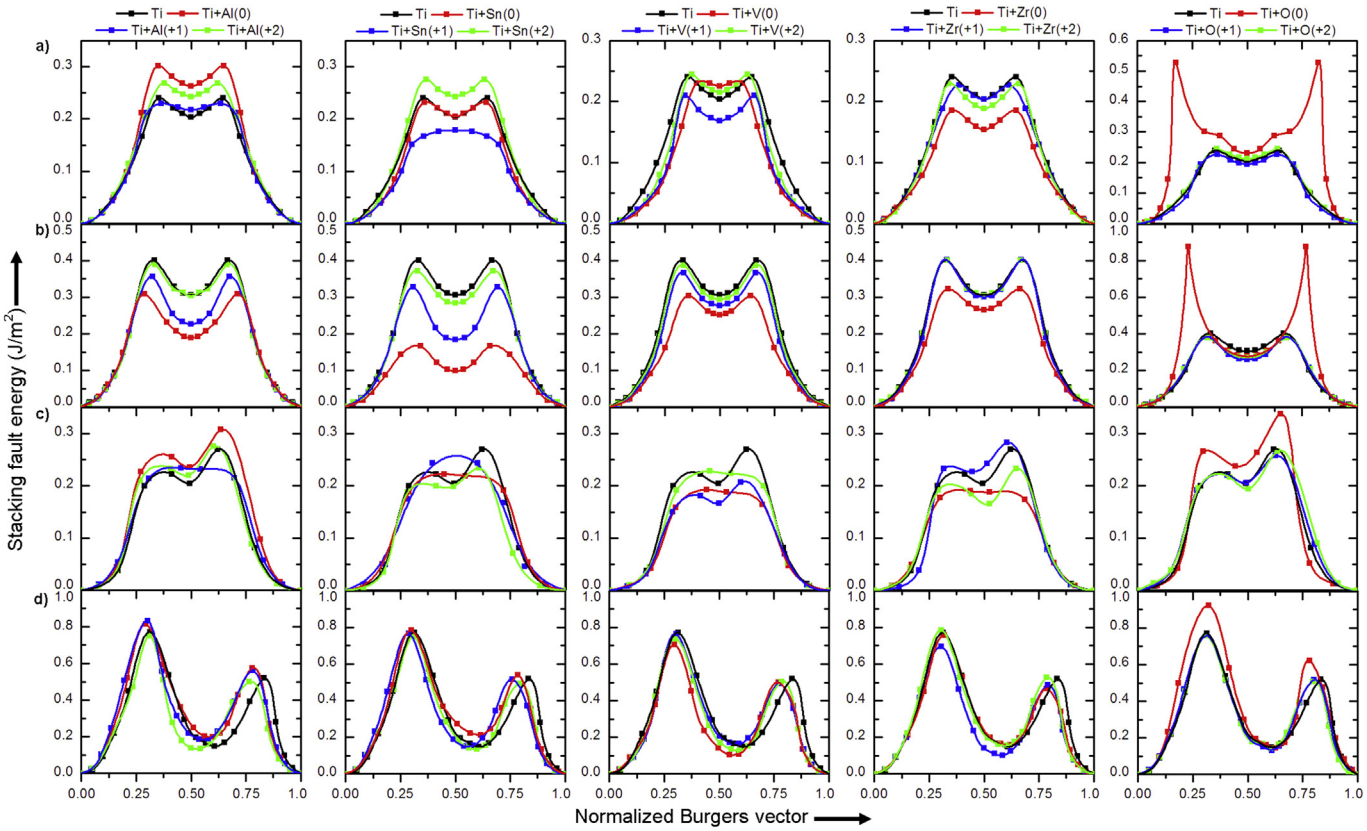

Fig. 1. GSFE curves of α-Ti and α-Ti+X alloys calculated for <a> prismatic (a), <a> basal (b), <a> pyramidal (c) and <c+a> pyramidal (d) slip modes. Various γ colors correspond to the location of the solutes (0,+1,+2 subsequent nearest positions relative to the glide plane): red (position 0), blue (+1) and green (+2). (For interpretation of the references to colour in this figure legend, the reader is referred to the web version of this article.)

Table 1
Averaged maximum restoring forces($\overline{F}_{max}$), unstable ($\overline{\gamma}_{USF}$) and stable ($\overline{\gamma}_{SF}$) stacking faults energies of pure Ti and its alloys (results obtained from 2×2 in-plane unit cell, 18 layers models). The forces and energies are given in meV/Å^3 and mJ/m^2, respectively. The available experimental and calculated data are denoted by superscript.

Slip mode	System	$\overline{F}_{max}$	$\overline{\gamma}_{USF}$	$\overline{\gamma}_{SF}$
<a> prismatic	Ti	22.5	240	203, 219^{DFT} [18], 220^{DFT} [26], 150^{exp} [45]
	Ti+Al	29.8	267	241
	Ti+Sn	25.3	229	209
	Ti+V	27.2	228	203
	Ti+Zr	19.4	214	182
	Ti+O	85.7	333	213
<a> basal	Ti	32.4	401	306, 292^{DFT} [26], 307^{DFT} [17], 319^{DFT} [43], 300^{exp} [44]
	Ti+Al	30.4	351	239
	Ti+Sn	24.5	289	189
	Ti+V	29.1	353	275
	Ti+Zr	31.2	375	290
	Ti+O	80.4	546	269
<a> pyramidal	Ti	28.0	270	205
	Ti+Al	31.0	272	229
	Ti+Sn	27.2	235	222
	Ti+V	22.5	209	193
	Ti+Zr	27.6	235	199
	Ti+O	32.6	287	221
<c+a> pyramidal	Ti	54.4	772	148
	Ti+Al	55.6	800	172
	Ti+Sn	46.6	767	166
	Ti+V	53.3	736	132
	Ti+Zr	45.8	746	140
	Ti+O	54.9	822	139

Dislocation nucleation is a highly dynamic process controlled by stress state and stress concentrators. Analyzing the results presented in Fig. 1 it is hard to predict how various positions of solutes will act on emission and dissociation of dislocations. However, 6 at% concentration of X, uniformly distributed within the crystal can be represented by the $2 \times 2 \times 2$ unit cell α-Ti structure (16 atoms) with one solute atom. In the above composition as well as for higher X concentrations, alloying elements will always interact with glide

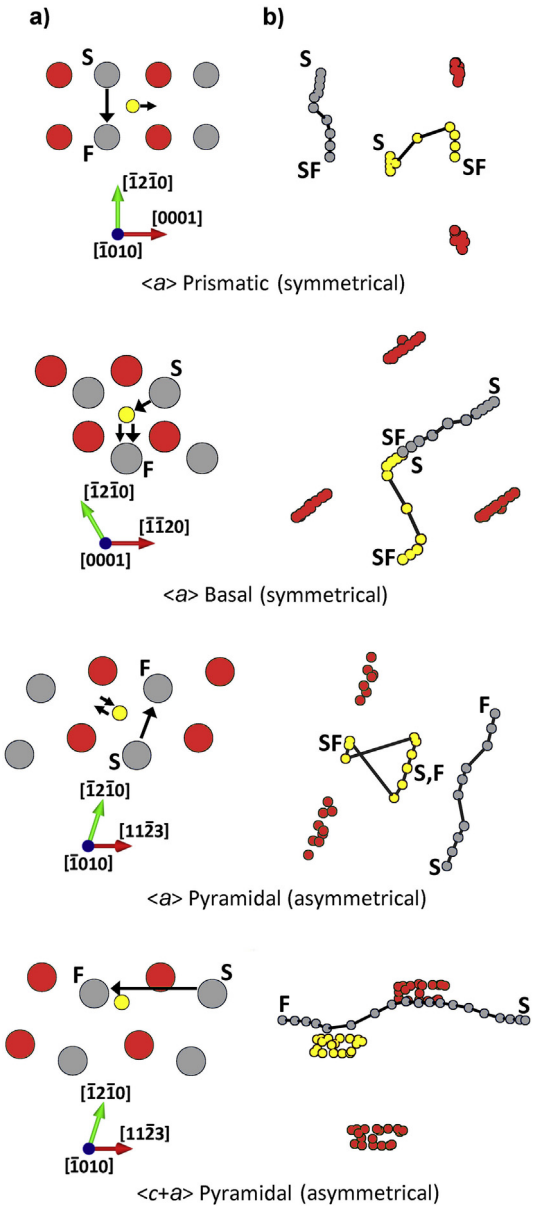

Fig. 2. Burgers and oxygen displacement vectors (black arrows) of four active α-Ti slip systems (a) and the GSFE-NEB slip trajectories (b). Red and grey circles denote atomic positions below and above the glide plane. The oxygen atoms are located in-glide plane site and marked by the yellow circles. "S", "F" and "SF" symbols indicate atomic positions at initial, final and stacking fault configurations. Glide planes in all figures are parallel to the drawing plane. To improve readability, trajectories of the symmetrical modes are plotted from "S" to "SF" configurations. (For interpretation of the references to colour in this figure legend, the reader is referred to the web version of this article.)

plane as O, +1 or +2 nearest neighbor. According to this fact the γ_{SF}, γ_{USF} and the maximum restoring forces (F_{max}) have been averaged as follows:

$$\overline{\gamma}_{SF,USF} = \frac{\gamma^{0}_{SF,USF} + \gamma^{+1}_{SF,USF} + \gamma^{+2}_{SF,USF}}{3}, \quad (1)$$

$$\overline{F}_{\max} = \frac{F^{0}_{\max} + F^{+1}_{\max} + F^{+2}_{\max}}{3}, \quad (2)$$

and the restoring forces are defined as [52]:

$$F(\delta) = \nabla[\gamma(\delta)] \quad (3)$$

In the above equations, δ is an arbitrary displacement vector, $\gamma^{0,+1,+2}_{SF,USF}$ and $F^{0,+1,+2}_{\max}$ are the stable, unstable stacking fault energies and maximum restoring forces calculated for 0, +1 and +2 solute position, respectively. The averaged values are listed in Table 1. It can be clearly seen that the $\overline{F}_{\max}$ of alloys with substitutional elements are markedly higher than those for pure α-Ti only for prismatic slip, while the average $\overline{\gamma}_{USF}$ are lower in most cases. Some discrepancies between $\overline{F}_{\max}$ and $\overline{\gamma}_{USF}$ values should be correlated with non-uniform electronic structures around solutes. Previous studies of point defects [35,53] revealed that alloying elements impair the host Ti–Ti or Mg–Mg bonds even at large distances. At the onset of the crystal slip, a part of the structure with weaker Ti–Ti bonds may be deformed, with lower elastic energy influencing the GSFE slope and F_{max} (see Ti+V prism slip in Fig. 1). Therefore, the correct prediction of dislocation nucleation in alloys necessitates simultaneous analysis of both F_{max} and γ_{USF} values, since the strengthening effect of solutes may be not visible from GSFE alone. Despite the weak impact of O on GSFEs in positions other than in-glide plane, interstitial O improves average $\overline{F}_{\max}$ and $\overline{\gamma}_{USF}$ of all modes.

The most pronounced variations of the GSFE parameters listed in Table 1 are associated with the reduction of γ_{SF} in the basal plane. The relative stability of prism, basal and pyramidal SF are extremely important for the core structure of 1/3<11$\bar{2}$0> dislocations [23,24]. The low energy of prism faults promotes planar cores, although basal and pyramidal spreading is also possible [25–28]. The impact of alloying solutes on relative SF stability has been determined on the basis of variation coefficient η:

$$\eta_{prism/\chi} = \left(\frac{\frac{\gamma_{SF}(Ti+X)_{prism}}{\gamma_{SF}(Ti+X)_{\chi}}}{\frac{\gamma_{SF}(Ti)_{prism}}{\gamma_{SF}(Ti)_{\chi}}} \right) - 1, \quad (4)$$

where χ expresses basal or pyramidal modes. The positive values of η indicate stabilization of χ SFs relative to prism one caused by the alloying elements. Fig. 3 shows strong stabilization of basal faults relative to prism one when *p* valence elements (Al, Sn, O) are added to Ti. Interestingly, transition elements (V, Zr) may differently interact with α-Ti lattice faults, which results from their valence structure (Zr has the same valence configuration as Ti). Moreover, interstitial O promotes <*c*+*a*> pyramidal faults and stabilizes/

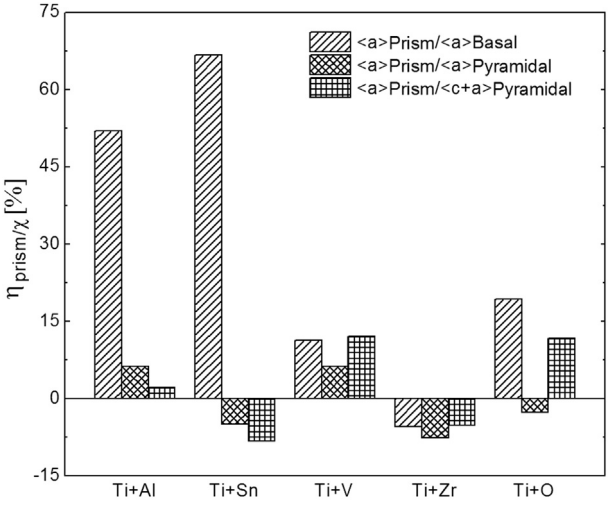

Fig. 3. Influence of alloying elements on relative stacking faults stability. Positive variation coefficient η [Eq. (4)] indicates destabilization of prism faults in favor of basal and pyramidal ones in the alloyed systems.

destabilizes basal/prism faults respectively, which is in accordance with the literature [17,18].

The data shown in Table 1 and Figs. 1 and 3 supply complex information about solution strengthening of α-Ti alloys. Basically, substitutional elements except Zr impede the nucleation of prismatic dislocations by improving $\overline{F}_{\max}$. An experimentally measured [5,6], explicit strengthening effect of *p* solutes (Al, Sn) is clearly related with the relative stability of basal and prismatic faults, which form the core structure of the 1/3<11$\bar{2}$0> dislocations [25–28]. M. Ghaziseidi et al. [26] noted that non planar 1/3<11$\bar{2}$0> core geometry (basal and pyramidal spreading) is sessile and reconstructs to prismatic configuration under applied strain, larger than those needed for planar core 1/3<11$\bar{2}$0>slipping. The results presented here suggest that the strengthening effect of *p* type alloying elements consist mainly in the stabilization of less mobile 1/3<11$\bar{2}$0> core geometries. The *d* type solutes (V, Zr) do not exhibit such features (Fig. 3) thus their strengthening ability is limited. It should also be noted that the strengthening effect of Zr is realized by γ_{SF} reduction. Due to lower γ_{SF}, dislocations are increasingly dissociated and their movement is restricted to individual planes. The determined values of USFEs suggest a similar energy barrier for dislocation nucleation in prismatic and <*a*> pyramidal modes in pure Ti, which is consistent with experiments [3]. Other studies reveal a note tendency to suppress prismatic and enhancement of basal dislocation emission in TiAl6V4 alloy, with a similar amount of <*a*> pyramidal dislocations to that in pure Ti, which again agrees with our predictions [8]. The relatively low impact of substitutional solutes on <*c*+*a*> pyramidal slip was also confirmed empirically [8].

The interstitial O has mixed impact on α-Ti stacking faults, but the strengthening effect of this element is primarily associated with the improvement of F_{max} and γ_{USF} leading to dislocation emission difficulties. The strong suppression of basal and prism dislocations was also reported by Conrad in single crystal CRSS measurements [5]. Nevertheless, basal and prism dislocations have been visible in polycrystalline α-Ti with relatively low (2000 ppm) O content [8]. It is thus important to determine the relation between strengthening ability and the concentration of solutes. To this end, additional GSFE computations were performed with 3 × 3 in-plane unit cell models (total X concentration about 0.6 at%) and X elements located directly in glide planes (configuration with the largest GSFE variations in Ti+O systems – Fig. 1).

To investigate the impact of solutes binding on GSFE, the changes in X–X interaction energies for various supercells size were calculated using the following equation [18]:

$$\Delta E^{b}_{0,USF,SF}(S_{2x2},S_{3x3}) = \frac{[E(S_{3x3}+X)-E(S_{3x3})]-[E(S_{2x2}+X)-E(S_{2x2})]}{4}, \quad (5)$$

where $S_{2\times2}$ and $S_{3\times3}$ denote size of the supercells, and $E(S_{2\times2(3\times3)}+X)$, $E(S_{2\times2(3\times3)})$ are energies of the structures with or without an alloying element, respectively. The 4 factor was introduced because in slab models each solute interacts with four neighbors (images). Since supercells used in calculations involve one solute atom, the exact X–X binding energy for individual structures is hard to predict. Instead, we used Eq. (5) to measure changes of X–X interaction (at unstrained ΔE^{b}_{0}, unstable ΔE^{b}_{USF} and metastable ΔE^{b}_{SF} SF configurations) when the distance between solutes goes from 2*a* to 3*a*. The proposed formula encompasses energies of models that differ in size, which generates approximately 1 meV errors related with computational methodology. The results of γ_{USF}, γ_{SF} and ΔE^{b} are presented in Fig. 4 and Table 2. As expected, the reduction of solutes concentration decreases the differences of GSFE parameters between alloyed and pure Ti. Fig. 4 displays a mild variation of γ_{SF} for all systems and an enormous dip in basal and prism γ_{USF} in Ti+O solutions. Small $\Delta E^{b}_{0,USF,SF}$ (Table 2) show comparable binding of substitutional elements at distance 2*a* and 3*a* in ground state and distorted configurations. Most of the energy variations are positive, indicating attraction to distance 2*a*. The Ti+O systems exhibit similar O–O interaction for both

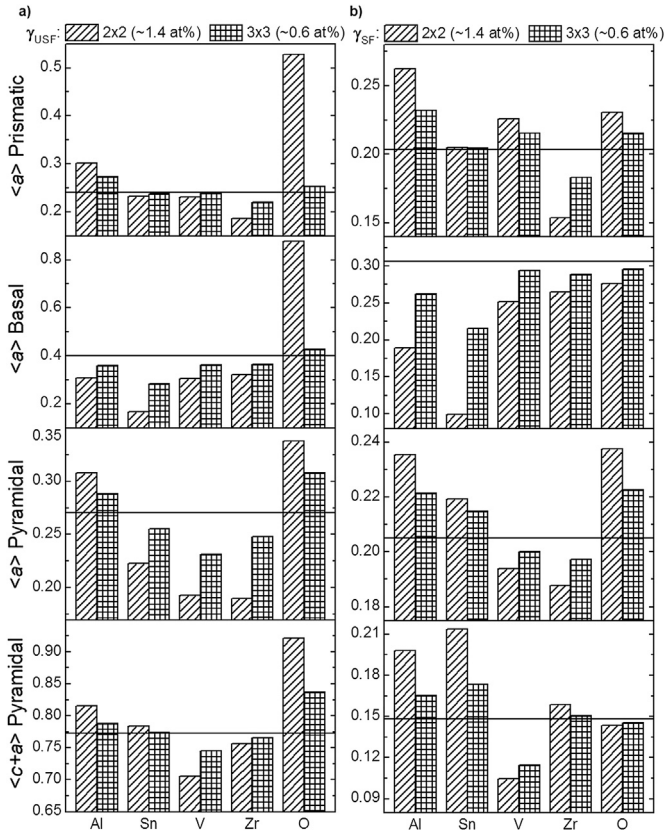

Fig. 4. Unstable (a) and stable (b) stacking fault energies of α-Ti alloys calculated for two X concentrations: 2 × 2 (~1.4 at% X) and 3 × 3 (~0.6 at% X) in-plane unit cell models. The solid black lines indicate reference pure Ti properties. The GSFE parameters are given in J/m^2.

Table 2
Changes in alloying elements binding energies calculated for 2 × 2 and 3 × 3 in-plane unit cell models. ΔE^{b}_{0}, ΔE^{b}_{USF} and ΔE^{b}_{SF} correspond to solutes interactions in unstrained, USF and SF structure configurations. Energies are in meV.

Slip mode	Element	ΔE^{b}_{0}	ΔE^{b}_{USF}	ΔE^{b}_{SF}
<*a*> prismatic	Al	13.0	19.5	18.2
	Sn	13.9	11.4	14.7
	V	7.6	8.7	12.1
	Zr	6.9	10.6	10.8
	O	6.6	**−197.2**	6.2
<*a*> basal	Al	4.4	−1.1	13.6
	Sn	15.5	−4.8	18.5
	V	−2.1	−2.7	11.6
	Zr	−9.9	−15.1	−7.9
	O	11.6	**−187.0**	15.2
<*a*> pyramidal	Al	9.6	13.6	16.9
	Sn	11.2	24.4	18.0
	V	4.5	−6.4	−1.2
	Zr	4.0	32.8	3.5
	O	9.7	26.3	16.4
<*c*+*a*> pyramidal	Al	9.6	6.8	−0.1
	Sn	11.2	5.9	4.8
	V	4.5	13.5	−19.9
	Zr	4.0	5.5	−1.2
	O	9.7	4.8	−1.1

structure size at initial and SF geometries (small ΔE_0^b and ΔE_{SF}^b), whereas large repulsive energies occur at distance 2*a* in unstable SF configurations for prismatic and basal mode (negative ΔE_{USF}^b). As described previously, O atoms located directly in particular glide planes migrate to a neighboring lower energy position, generating local structure distortion which depends on transition geometry. The computed ΔE_{USF}^b indicate that distance 2a is insufficient to inhibit the additional elastic deformation in basal and prismatic mode leading to strong repulsive force and increase in the energy barrier for dislocation nucleation. Due to this issue, the impact of isolated O on GSFE curves of α-Ti should be computed with at least 3×3 in-plane unit cell models, which greatly reproduce the essential reduction of <*c*+*a*> pyramidal dislocation emission responsible for the brittleness of hexagonal Ti+O solutions (absence of glide modes which can accommodate deformation in *c* direction) [8]. Nevertheless, the calculations performed with smaller supercells revealed the explicit role of structure relaxation during oxygen migration. All additional lattice distortions existing in the vicinity of the dislocation cores will therefore improve energy barrier for O migration compared to the ideal shearing case.

The results of ΔE^b show that the 2×2 in-plane unit cell models are appropriate for the GSFE calculations of substitutional Ti alloys due to solute self interaction near to those obtained for 3×3 in-plane structures (low ΔE^b). The binding energies in the order of tens meV occur even at great X–X distances, as was calculated lately [35], and should not be treated as a drawback of the slab model approach.

The γ curves plotted in Fig. 1 change non linearly with the position of the solutes. However, oxygen influences GSFE primarily when the interstitial atom is located directly within the glide plane indicating the short distance of effective O − slip plane interaction, although the other elements placed even at +2 site alter GSFE. It is thus justified to determine the critical separation distance at which substitutional elements do not affect GSFE. To this end, SFEs were computed in the range of 0 to +6 X position and the results obtained are presented in Fig. 5. It should be noted that these calculations were performed with the 2×2 in-plane unit cell and 26 layers models to prevent X interaction with free surfaces. The adoption of larger supercells size results in maximum 2% variations of SFEs compared to the original 18 atomic layers structures utilized for full GSFE computations. From the results obtained it can be concluded that the effective SF–X interaction range depends strongly on the slip system, i.e. substitutional solutes interplay with basal SF only at 0, +1 positions and up to +4, +5 sites in other modes. The active α-Ti slip systems may be ordered according to the increasing effective interaction range with substitutional solutes as follows: <*a*> basal, <*c*+*a*> pyramidal, <*a*> prismatic, <*a*> pyramidal.

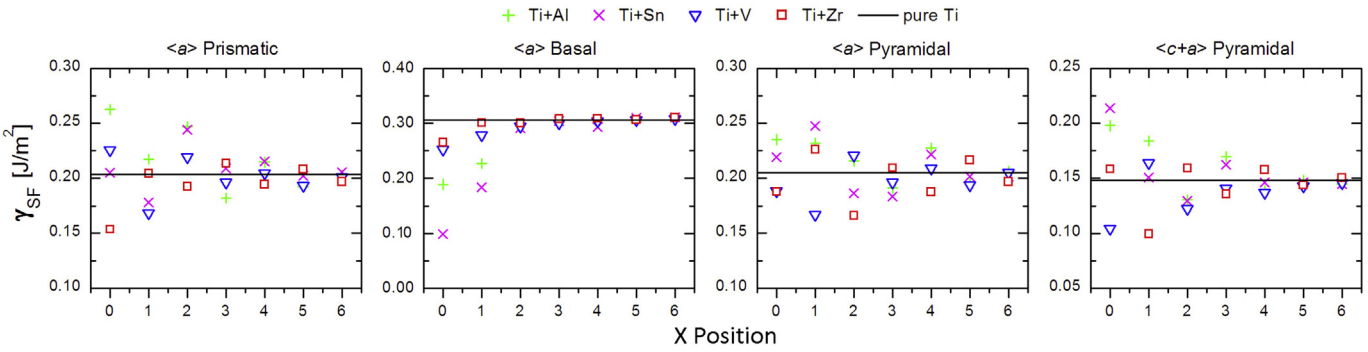

Fig. 5. Stacking fault energies of considered α-Ti alloys as a function of subsequent X (substitutional element) position relative to the glide plane. 0 and 6 correspond to X located in-glide plane and 6 atomic planes below, respectively.

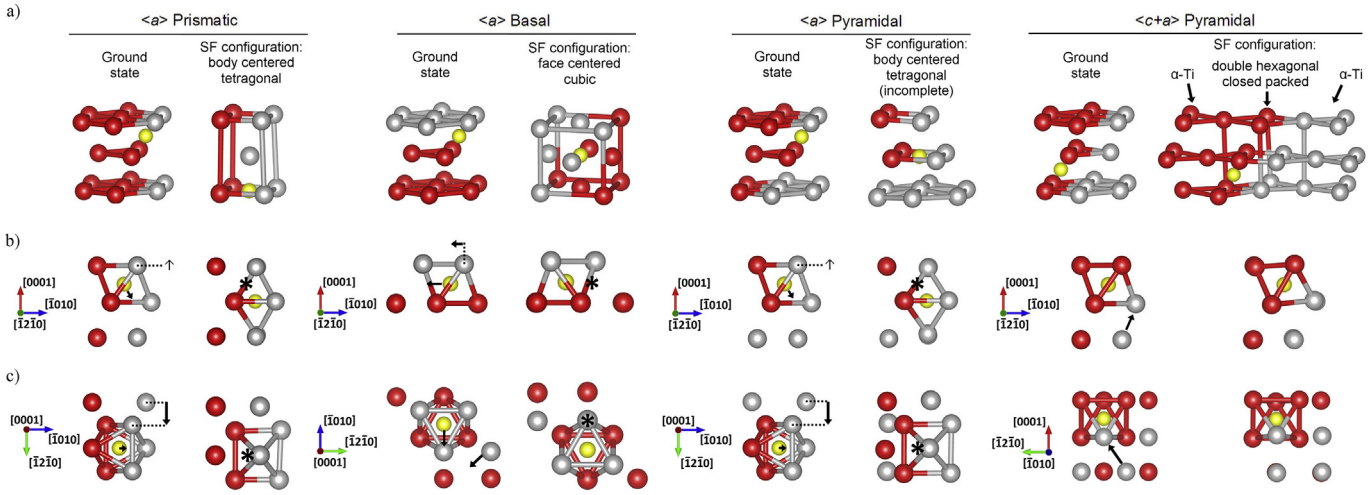

Fig. 6. Migration of interstitial O (yellow spheres) during SF formation. Red and gray spheres represent sessile and slipping Ti atoms, respectively. (a) O position in hcp and SF crystal structure (in pyramidal modes interstitial elements are located at the interface of hcp and SFs lattice). Front (b) and side (c) views of interstitial site geometries at ground state and SF configurations. Oxygen displacements and Burgers vectors of partial dislocations are marked by black arrows (thick arrow symbol "↑" indicates motion in direction perpendicular to the figure plane). Initial O sites are also denoted by "*". (For interpretation of the references to colour in this figure legend, the reader is referred to the web version of this article.)

3.2. Electronic and atomic structures of α-Ti stacking faults

To clarify the distinct impact of O on GSFE curves, the slip geometries with interstitial site reconfiguration is shown in Fig. 6. It can be seen that in all <a> type slip systems an initial octahedral site is unavailable when SF geometry is reached. The prismatic and <a> pyramidal SFs form an equivalent, bcc like octahedral site resulting in similar γ_{SF} values. Nonetheless, the markedly different energy barriers γ_{USF} of these transitions arise from various glide plane types (see position of the gray spheres in Fig. 6). In basal slip, continuous octahedral → tetrahedral and tetrahedral → octahedral gap reconfigurations take place. An

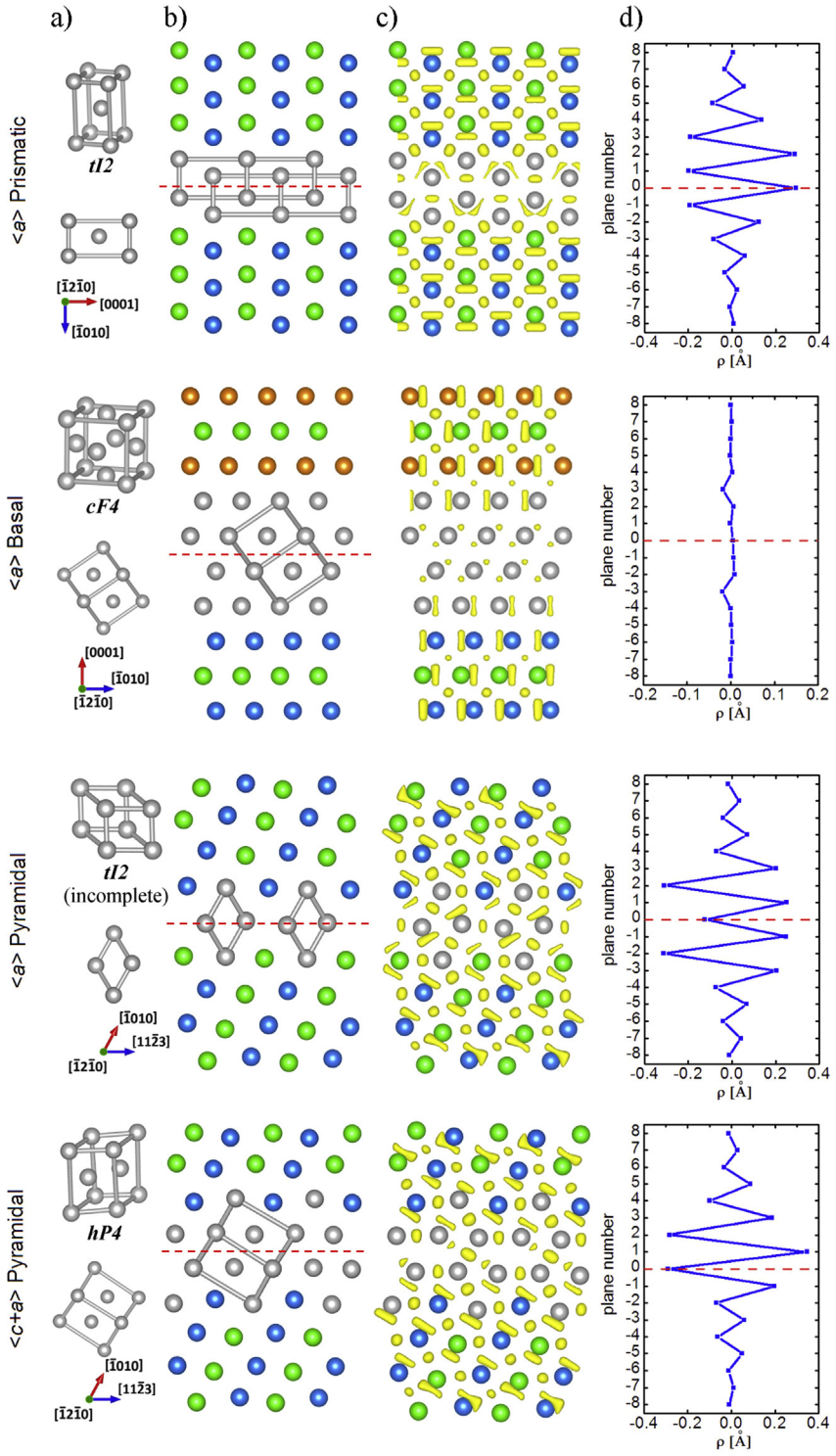

Fig. 7. Hexagonal Ti stacking faults: unit cell, Pearson number and orientation relative to host crystal (a), SFs structure arrangement (b), atomic bond patterns (yellow zones indicate ELF isosurfaces) (c) and interplanar distance distortion plots (d). The gray spheres depict atoms belonging to SF regions while blue, green and orange ones denote A, B and C sequence of basal planes in unaltered sections of the crystal. Slip planes are marked by the red dashed lines. The ELF isosurface level is equal to 0.7 in all cases. (For interpretation of the references to colour in this figure legend, the reader is referred to the web version of this article.)

interstitial tetrahedral position of O is unstable and spontaneously transforms to the hexahedral site, 1.19 eV higher in energy than the octahedral one [48]. This large energy difference provides the driving force for O migration into the newly created, favorable site. Migrations of O into other octahedral positions (e.g. one atomic layer below) were calculated as well, but the energy barriers in each case were about 1.8 eV higher. The single <c+a> pyramidal glide does not alter the position of O, since only one atom forming the octahedral gap is slipping. An essential improvement of γ_{USF} caused by O in this mode arises from extensive relaxation of Ti atomis during the slip [4], which is hindered by strong Ti–O bonding.

As presented in Fig. 1, the position of the substitutional elements strongly affects the shape of the GSFEs. The relation above may be elucidated on the basis of the atomic and electronic structure of four α-Ti SFs shown in Fig. 7. Although the SF transition is realized by the crystal slip in one glide plane, the created structures involve a few atomic layers. The prismatic and <a> pyramidal faults consist of similar body centered tetragonal cells, which in pyramidal mode are incomplete (lack of the third (001) tetragonal plane). It is worth noting that the same <a> pyramidal SF configuration was also found recently in zirconium [54,55]. The other basal and <c+a> pyramidal SF forms full fcc and dhcp structures, respectively. The bonding pattern presented in Fig. 7c was reproduced utilizing electron localization function (ELF). Becke and Edgecombe [56] introduced ELF as a function describing the probability of finding two electrons with the same spin in space. ELF is normalized to the range of 0–1; ELF = 0.5 indicates a homogeneous electron gas, whereas values close to 1 represent a highly localized covalent or ionic interactions [57]. ELF isosurfaces in Fig. 7c were adjusted to 0.7 and display covalent regions of bonds. It can be clearly seen that the bond array within all SF structures differs from those in α-Ti due to the separate coordination number. Moreover, in all cases the amount of strong covalent bonds decrease, as is manifested by smaller and less directional ELF zones. The most pronounced transition from covalent to metallic bonding takes place in basal SF, which results in large γ_{SF} (pure Ti) values of this system. Recent investigations revealed that α-Ti solutes have better solubility in twin boundaries (TB) than in bulk, due to the excess volume of the twin-bulk structure interface [19]. Since both TB and SF exhibit many common features, α-Ti SFs interplanar distance distortion ρ (difference of interplanar distance between distorted and unstrained crystal) is plotted in Fig. 7d. The prismatic and pyramidal fault structures display marked ρ variations, while the basal SF configuration introduces only slight distortion of the crystal lattice – the basal SF consists of close packed planes with alter sequence (ABABCACA...) whereas in other modes, these high density atomic planes are locally shifted (a square instead of a triangular atomic pattern is formed) generating extensive elastic displacement field. This unique feature, together with the distinct character of the bonds, explains the reduction of basal γ_{SF} in all substitutional solutions (see Fig. 1). Alloying elements placed in the α-Ti lattice produce local structure deformation and excess energy. Deformation created by solute in basal SF can be easily accommodated, owing to the weak metallic bond array occurring in its vicinity. An additional lattice deformation and different coordination number available in other types of SFs (Fig. 7d) may prevent relaxation improving γ_{SF} values as presented in Fig. 1.

To evaluate the impact of lattice relaxation around solutes on SFE, the total interplanar distance distortions $\Sigma\rho$ were computed as follows:

$$\sum \rho = \sum_{i=1}^{n} \rho_i = \left|d_1^{SF}(Ti+X) - d_1^{ground}(Ti+X)\right| + \left|d_2^{SF}(Ti+X) - d_2^{ground}(Ti+X)\right| + \ldots + \left|d_n^{SF}(Ti+X) - d_n^{ground}(Ti+X)\right|, \quad (6)$$

where $d_i^{SF}(Ti{+}X)$ and $d_i^{ground}(Ti{+}X)$ are the interplanar distances in the alloyed SFs and ground state solutions, respectively. The summation of ρ is performed over $n = 17$ interplanar distances. The $\Sigma\rho$ was calculated for Ti+Al(Sn) basal and prismatic modes (due to the large number of systems considered, those with the largest γ_{SF} variations were chosen) and plotted in Fig. 8. It is clearly visible that γ_{SF} tends to change linearly with $\Sigma\rho$ which confirms that SFE in the alloyed systems are deeply correlated with SF structure relaxation capability. The $\gamma_{SF} = f(\Sigma\rho)$ line slope is positive or negative since point defects may locally collapse or expand the host crystal. Some discrepancies from the linear manner are expected due to the different bond pattern occurring in 0, +1 and +2 solute position, as presented in Fig. 8b,c.

The atomic and electronic configurations of SFs displayed in Figs. 7 and 8 show that the faulted parts of the crystal have a highly non-uniform structure. Their thickness, equal to a few atomic layers, results in continuous structure distortion at the SF-bulk α-Ti interface as well as in the SF region. The strong impact of the position of X solutes on GSFE is the effect of the above SF features. The results of calculations performed answers the outstanding question: Why/how alloying elements may improve or reduce SFE of the material? Transition of the character of bonds (from moderate covalent to metallic) and their disorder facilitate structure relaxation in the point defect vicinity (relative to the ideal α-Ti lattice) enabling SFE reduction. On the other hand, interplanar distance

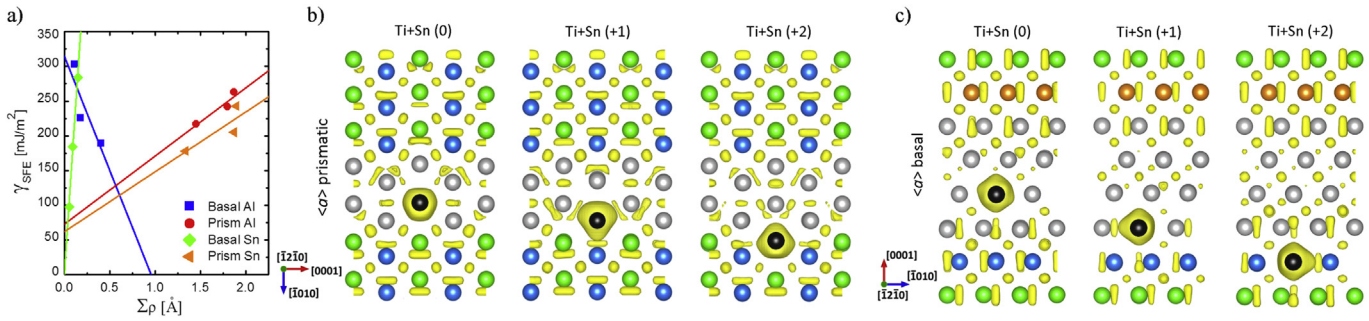

Fig. 8. SFE vs total interplanar distance distortion plot for prism and basal modes in Ti+Al and Ti+Sn alloys (a). ELF distribution of the selected SF with Sn atoms (black spheres) located at various positions relative to the glide plane (b,c). Distinct/slight changes of the bond pattern in the alloyed prismatic/basal SF correspond to deviations from linear dependencies shown in (a). Representations of atoms (colors) and isosurface level are analogous to those used in Fig. 7. (For interpretation of the references to colour in this figure legend, the reader is referred to the web version of this article.)

distortion, various coordination number and different X solubility in SF structures may prevent relaxation, increase the energy of the Ti-X bonds and total SFE. These two competing effects are mutually linked and determine SFEs of the hexagonal Ti alloys.

4. Conclusions

The article provides the results of GSFE and restoring forces computations performed for a series of hexagonal Ti+X (X = Al, Sn, V, Zr and O) alloys. The calculation methodology takes into account elastic deformation of the crystal by allowing full atomic relaxation and provides the minimum energy path of the γ curve thanks to utilizing the combined GSFE-NEB approach [4]. The conclusions of this paper are as follows:

- The impact of individual alloying elements on GSFE parameters (F_{max}, γ_{USF} and γ_{SF}) depends strongly and non linearly on their position relative to glide planes.
- The solution strengthening associated with dislocation nucleation in the alloyed systems should be evaluated on the basis of both F_{max} and γ_{USF} due to the electronic structure variations influencing the GSFE slope even for similar γ_{USF} values.
- The solution strengthening of Ti+X alloys is realized through three distinct mechanisms related with the valence structure and lattice position (substitutional or interstitial) of X: (I) the p elements (Al and Sn) impede prismatic dislocation emission and reduce/improve basal/prismatic faults energy, respectively. This effect stabilizes the less mobile, non-planar core of screw 1/3<11$\bar{2}$0> dislocations [26,27] leading to the significant strengthening of α-Ti; (II) the (d) solutes (V, Zr) may hinder the prismatic dislocation emission and reduce γ_{SF} in other modes. The impact of V and Zr on prismatic screw dislocations is less pronounced and therefore their strengthening ability is limited; (III) interstitial oxygen suppresses dislocation emission in all slip modes by enhancing F_{max} and γ_{USF} values. Nevertheless, this effect is observed only when O is located directly in the glide plane.
- The robust strengthening of Ti—O solutions originates from O migration to the newly created interstitial site formed during <a> type crystal slip. The limitation of <c+a> pyramidal dislocations nucleation is the effect of the structure stiffening provided by Ti—O bonds, preventing extensive atomic relaxation occurring in this mode [4]. The above mechanisms are strongly related with O concentration: basal and prismatic dislocations nucleation is blocked at high O content, while <c+a> pyramidal dislocations emission is reduced even for low O amounts.
- α-Ti stacking faults created after partial dislocation emission have face centered cubic (basal slip), body centered tetragonal (prismatic and <a> pyramidal slip) and double hexagonal (<c+a> pyramidal slip) configurations spanning over a few atomic planes. The low thickness of SFs (SF/bulk α-Ti interfaces interaction, various coordination number and volume of both phases) results in their non-uniform electronic structure and lattice distortion. Due to the listed structural inhomogeneities, SF regions should not be treated as a perfect isolated phase.
- Alloying elements may reduce or improve energies of individual stacking faults in α-Ti. In general, SFEs essentially depend on the relaxation ability of the faulted regions. The accommodation of lattice deformation caused by the presence of alloying solutes is facilitated by atomic bond disorder and their transition to explicitly metallic at SF configurations. However, interplanar distance distortion and different solute solubility within SF structures improve total SFE. Various X positions relative to the glide plane determine the diverse balance of the above effects, resulting in different SFE values.

Acknowledgments

This work was supported by Structural Funds in the Operational Programme - Innovative Economy (IE OP) financed from the European Regional Development Fund under Grant No. POIG.01.01.02-00-015/08-00. Computing resources were provided by HPC facilities of the Interdisciplinary Center for Mathematical and Computational Modelling at Warsaw University under grant G44-6.

References

[1] S. Sandlöbes, S. Zaefferer, I. Schestakow, S. Yi, R. Gonzalez-Martinez, On the role of non-basal deformation mechanisms for the ductility of Mg and Mg–Y alloys, Acta Mater. 59 (2011) 429.
[2] S. Bin, L. Shufeng, I. Hisashi, U. Junko, K. Katsuyoshi, Fabrication of high-strength Ti materials by in-process solid solution strengthening of oxygen via P/M methods, Mater. Sci. Eng. A 563 (2013) 95.
[3] J. Gong, A.J. Wilkinson, Anisotropy in the plastic flow properties of single-crystal α titanium determined from micro-cantilever beams, Acta Mater. 57 (2009) 5693.
[4] P. Kwaśniak, P. Śpiewak, H. Garbacz, K.J. Kurzydłowski, Plasticity of hexagonal systems: split slip modes and inverse Peierls relation in α-Ti, Phys. Rev. B 89 (2014) 144105.
[5] H. Conrad, Effect of interstitial solutes on the strength and ductility of titanium, Prog. Mater. Sci. 26 (1981) 123.
[6] E.W. Collings, H.L. Gegel, Physics of Solid Solution Strengthening, Plenum Press, New York, 1975.
[7] A.T. Churchman, The slip modes of titanium and the effect of purity on their occurrence during tensile deformation of single crystals, Proc. R. Soc. Lond. A 226 (1954) 216.
[8] S. Zaefferer, A study of active deformation systems in titanium alloys: dependence on alloy composition and correlation with deformation texture, Mater. Sci. Eng. A 344 (2003) 20.
[9] J.W. Christian, V. Vitek, Dislocations and stacking faults, Rep. Prog. Phys. 33 (1970) 307.
[10] B. Joós, Q. Ren, M.S. Duesbery, Peierls-Nabarro model of dislocations in silicon with generalized stacking-fault restoring forces, Phys. Rev. B 50 (1994) 5890.
[11] B. Joós, M.S. Duesbery, The Peierls stress of dislocations: an analytic formula, Phys. Rev. Lett. 78 (1997) 266.
[12] V.V. Bulatov, E. Kaxiras, Semidiscrete variational Peierls framework for dislocation core properties, Phys. Rev. Lett. 78 (1997) 4221.
[13] G. Lu, N. Kioussis, V.V. Bulatov, E. Kaxiras, Generalized-stacking-fault energy surface and dislocation properties of aluminium, Phys. Rev. B 62 (2000) 3099.
[14] E. Tadmor, S. Hai, A Peierls criterion for the onset of deformation twinning at a crack tip, J. Mech. Phys. Solids 51 (2003) 765.
[15] U. Waghmare, E. Kaxiras, M.S. Duesbery, Modelling brittle and ductile behavior of solids from first-principles calculations, Phys. Status Sol. (b) 217 (2000) 545.
[16] S. Yip, Handbook of Materials Modelling, Springer, New York, 2005.
[17] P. Kwasniak, M. Muzyk, H. Garbacz, K.J. Kurzydlowski, Influence of C, H, N, and O interstitial atoms on deformation mechanism in titanium—first principles calculations of generalized stacking fault energy, Mater. Lett. 94 (2013) 92.
[18] M. Ghazisaeidi, D.R. Trinkle, Interaction of oxygen interstitials with lattice faults in Ti, Acta Mater. 76 (2014) 82.
[19] A. Kumar, J. Wang, C.N. Tomé, First-principles study of energy and atomic solubility of twinning-associated boundaries in hexagonal metals, Acta Mater. 85 (2015) 144.
[20] S. Naka, A. Lasalmonie, P. Costa, L.P. Kubin, The low-temperature plastic deformation of α-titanium and the core structure of a-type screw dislocations, Philos. Mag. A 57 (1988) 717.
[21] S. Naka, A. Lasalmonie, Prismatic slip in the plastic deformation of α-Ti single crystals below 700 K, Mater. Sci. Eng 56 (1982) 19.
[22] M. Biget, G. Saada, Low-temperature plasticity of high-purity α-titanium single crystals, Philos. Mag. A 59 (1989) 747.
[23] E. Clouet, Screw dislocation in zirconium: an ab initio study, Phys. Rev. B 86 (2012) 144104.
[24] B. Legrand, Relations entre la structure électronique et la facilité de glissement dans les métaux hexagonaux compacts, Philos. Mag. B 49 (1984) 171.
[25] N. Tarrat, M. Benoit, J. Morillo, Core structure of screw dislocations in hcp Ti: an ab initio DFT study, Int. J. Mater. Res. 100 (2009) 329.
[26] M. Ghazisaeidi, D.R. Trinkle, Core structure of a screw dislocation in Ti from density functional theory and classical potentials, Acta Mater. 60 (2012) 1287.
[27] S.I. Rao, A. Venkateswaran, M.D. Letherwood, Molecular statics and molecular dynamics simulations of the critical stress for motion of a/3 <11$\bar{2}$0> screw dislocations in a-Ti at low temperatures using a modified embedded atom method potential, Acta Mater. 61 (2013) 1904.
[28] N. Tarrat, M. Benoit, D. Caillard, L. Ventelon, N. Combe, J. Morillo, Screw dislocation in hcp Ti : DFT dislocation excess energies and metastable core structures, Model. Simul. Mater. Sci. Eng 22 (2014) 055016.
[29] Z. Wang, M. Saito, K.P. McKenna, Y. Ikuhara, Polymorphism of dislocation core structures at the atomic scale, Nat. Commun. 5 (2014) 3239.

[30] S. Wang, N. Hashimoto, S. Ohnuki, Hydrogen-induced change in core structures of {110}[111] edge and {110}[111] screw dislocations in iron, Sci. Rep. 3: 2760, DOI: 10.1038/srep02760.
[31] G. Kresse, J. Hafner, Ab initio molecular dynamics for liquid metals, Phys. Rev. B 47 (1993) 558.
[32] G. Kresse, J. Furthmüller, Efficient iterative schemes for ab initio total-energy calculations using a plane-wave basis set, Phys. Rev. B 54 (1996) 11169.
[33] P.E. Blöchl, Projector augmented-wave method, Phys. Rev. B 50 (1994) 17953.
[34] P. Kwasniak, M. Muzyk, H. Garbcz, K.J. Kurzydlowski, Influence of oxygen content on the mechanical properties of hexagonal Ti − First principles calculations, Mater. Sci. Eng. A 590 (2014) 74.
[35] P. Kwasniak, M. Muzyk, H. Garbcz, K.J. Kurzydlowski, Clustering of O–X, X = (Ag, Al, Ga, Sn, Sc, Zn, Zr) point defects in hexagonal Ti: formation mechanism and ductility variations, Mater. Chem. Phys. 154 (2015) 137.
[36] J.P. Perdew, K. Burke, M. Ernzerhof, Generalized gradient approximation made simple, Phys. Rev. Lett. 77 (1996) 3865.
[37] H.J. Monkhorst, J.D. Pack, Special points for Brillouin-zone integrations, Phys. Rev. B 13 (1976) 5188.
[38] G. Lutjering, J. Williams, Titanium, Springer-Verlag, Berlin, 2003.
[39] D. Sheppard, R. Terrell, G. Henkelman, Optimization methods for finding minimum energy paths, J. Chem. Phys. 128 (2008) 134106.
[40] D. Sheppard, G. Henkelman, Paths to which the nudged elastic band converges, J. Comput. Chem. 32 (2011) 1769.
[41] G. Henkelman, B.P. Uberuaga, H. Jónsson, A climbing image nudged elastic band method for finding saddle points and minimum energy paths, J. Chem. Phys. 113 (2000) 9901.
[42] J.R. Rice, Dislocation nucleation from a crack tip: an analysis based on the Peierls concept, J. Mech. Phys. Solids 40 (1992) 239.
[43] A. Poty, J.M. Raulot, H. Xu, J. Bai, C. Schuman, J.S. Lecomte, M.J. Philippe, C. Esling, Classification of the critical resolved shear stress in the hexagonal-close-packed materials by atomic simulation: application to α-zirconium and α-titanium, J. Appl. Phys. 110 (2011) 014905.
[44] P.G. Partridge, The crystallography and deformation modes of hexagonal close-packed metals, Metall. Rev. 118 (1967) 169.
[45] E.S. Fisher, C.J. Renken, Single-crystal elastic moduli and the hcp → bcc transformation in Ti, Zr, and Hf, Phys. Rev. 135 (1964) A482.
[46] C. Wang, H.-Y. Zhang, H.-Y. Wang, G.-J. Liu, Q.-C. Jiang, Effects of doping atoms on the generalized stacking-fault energies of Mg alloys from first-principles calculations, Scr. Mater. 69 (2013) 445.
[47] R.G. Henning, D.R. Trinkle, J. Bouchet, S.G. Srinivasan, R.C. Albers, J.W. Wilkins, Impurities block the α to ω martensitic transformation in titanium, Nat. Mater. 4 (2005) 129.
[48] H.H. Wu, D.R. Trinkle, Direct diffusion through interpenetrating networks: oxygen in titanium, Phys. Rev. Lett. 107 (2011) 045504.
[49] P.G. Oberson, S. Ankem, Why twins do not grow at the speed of sound all the time, Phys. Rev. Lett. 95 (2005) 165501.
[50] P.G. Oberson, Z.W. Wyatt, S. Ankem, Modeling interstitial diffusion controlled twinning in alpha titanium during low-temperature creep, Scr. Mater. 65 (2011) 638.
[51] Q. Yu, L. Qi, T. Tsuru, R. Traylor, D. Rugg, J.W. Morris, M. Asta, D.C. Chrzan, A.M. Minor, Origin of dramatic oxygen solute strengthening effect in titanium, Science 347 (2015) 635.
[52] J. Hirth, J. Lothe, Theory of Dislocation, second ed., Wiley, New York, 1992.
[53] J. Han, X.M. Su, Z.H. Jin, Y.T. Zhu, Basal-plane stacking-fault energies of Mg: a first-principles study of Li- and Al-alloying effects, Scr. Mater. 64 (2011) 693.
[54] N. Chaari, E. Clouet, D. Rodney, First-principles study of secondary slip in zirconium, Phys. Rev. Lett. 112 (2014) 075504.
[55] N. Chaari, E. Clouet, D. Rodney, First order pyramidal slip of 1/3 $<1\bar{2}10>$ screw dislocations in zirconium, Metall. Mater. Trans. A 45 (2014) 5898.
[56] A.D. Becke, K.E. Edgecombe, A simple measure of electron localization in atomic and molecular systems, J. Chem. Phys. 92 (1990) 5397.
[57] B. Slivi, A. Savin, Classification of chemical bonds based on topological analysis of electron localization functions, Nature 371 (1994) 683.